Organic photonic bandgap microcavities doped with semiconductor nanocrystals for room-temperature on-demand single-photon sources

Svetlana G. Lukishova [a]; Luke J. Bissell [a]; Vinod M. Menon [b]; Nikesh Valappil [b]; Megan A. Hahn [c]; Chris M. Evans [c]; Brandon Zimmerman [a]; Todd D. Krauss [c]; C. R. Stroud Jr [a]; Robert W. Boyd [a]

[a] The Institute of Optics, University of Rochester, Rochester, NY, USA [b] Department of Physics, Queens College-CUNY, Flushing, NY, USA [c] Department of Chemistry, University of Rochester, Rochester, NY, USA

PLEASE SCROLL DOWN FOR ARTICLE

Taylor & Francis
Taylor & Francis Group

Organic photonic bandgap microcavities doped with semiconductor nanocrystals for room-temperature on-demand single-photon sources

Svetlana G. Lukishova[a]*, Luke J. Bissell[a], Vinod M. Menon[b], Nikesh Valappil[b], Megan A. Hahn[c], Chris M. Evans[c], Brandon Zimmerman[a], Todd D. Krauss[c], C.R. Stroud Jr[a] and Robert W. Boyd[a]

[a]*The Institute of Optics, University of Rochester, Rochester, NY USA;* [b]*Department of Physics, Queens College – CUNY, Flushing, NY USA;* [c]*Department of Chemistry, University of Rochester, Rochester, NY USA*

We report the first experimental observation of fluorescence from *single* semiconductor nanocrystals (colloidal quantum dots) in microcavities. In these room-temperature experiments we observed photon antibunching from single CdSe nanocrystals doped into a chiral one-dimensional photonic bandgap liquid-crystal microcavity. The chirality resulted in high-purity, circular polarization of definite handedness of the emitted single photons. We also report the fabrication of chiral microcavities for telecom wavelengths doped with PbSe nanocrystals as well as a solution-processed-polymer microcavity with a defect layer doped with CdSe nanocrystals between two distributed Bragg reflectors. These systems with their low host fluorescence background are attractive for on-demand single-photon sources for quantum information and communication.

Keywords: single-photon sources; colloidal quantum dots; microcavities

1. Introduction

The development of on-demand single-photon sources (SPSs) with photons exhibiting antibunching has recently been of significant interest for their applications in quantum cryptography [1–4]. A desirable feature for a SPS is photon polarization, since in the case of single photons with definite polarization, the quantum cryptography system's efficiency will be twice that of an unpolarized SPS.

Room-temperature SPSs based on colloidal semiconductor quantum-dot (QD) fluorescence [5,6] are very promising because of higher QD photostability at room temperature than that of conventional dyes, and relatively high quantum yield (up to ∼100%). Recently, electrically driven light emission from a *single* colloidal QD at room temperature was obtained [7], opening up the possibility for electrical pumping of an SPS on demand, based on colloidal QDs. At the same time, colloidal QDs can be dissolved/dispersed in various hosts, e.g. photonic crystal microcavities, from solution. Placed into a microcavity environment, the QD spontaneous emission rate can be enhanced via the Purcell effect [4]. The cavity geometry can also influence QD polarization.

In spite of the well-developed microcavity fabrication techniques [8], and wide use of these techniques for heterostructured QDs operating at cryogenic temperatures, e.g. [4,9], there are only few reports of doping *colloidal* QDs into microcavities. For instance, Poitras et al. [10] demonstrated spontaneous emission enhancement by a factor of 2.7 from CdSe QDs embedded in a half-wavelength one dimensional cavity sandwiched between two distributed Bragg reflectors (DBR). The DBRs were prepared using sputter deposition of TiO_2-SiO_2 quarter-wavelength thick layers. Kahl et al. [11] started with the same approach, but also used a focused ion beam to etch micropillar microcavities of both round and elliptical cross-section from a planar cavity. Martiradonna et al. [12] combined the DBR technique prepared by e-beam evaporation of TiO_2-SiO_2 layers with imprint lithography of a defect layer. Lodahl et al. [13] embedded CdSe QDs into a titania inverse opal photonic crystal and observed both inhibition and enhancement of decay rates. Fushman et al. [14] mapped cavity resonances of PbS QDs in an AlGaAs membrane using QD fluorescence. Wu et al. [15] achieved efficient coupling of 1.5-μm emission from PbSe QDs to a Si-based photonic-crystal-membrane microcavity with a Purcell factor of 35. In [16], Bose et al. reported weak coupling of PbS QDs with the same Si-based microcavity. In addition, Hoogland et al. [17] reported PbS QD 1.5-μm lasing of whispering gallery modes in a microcapillary resonator, and Barrelet et al. [18] studied CdS QDs in nanowire one-dimensional photonic crystal structures.

*Corresponding author. Email: sluk@lle.rochester.edu

It should be noted that no data exist in the literature on the fluorescence of room-temperature, *single* colloidal QDs embedded in the microcavity environment, nor on preserving fluorescence antibunching of single colloidal QDs in the cavity materials. All results on SPSs based on QDs in microcavities, see, e.g. [4,9], are reported for heterostructured QDs at cryogenic temperatures.

We describe here the results of doping single colloidal semiconductor QDs in two types of organic 1-D photonic bandgap microcavities which permit us to use single colloidal QDs directly from a solution: (1) chiral microcavity made of monomeric and/or oligomeric planar-aligned cholesteric liquid crystals (CLCs) [19–21] and (2) polymer microcavity with a defect layer between two DBRs [22–23]. These two types of microcavity are robust and simple in fabrication.

We report the first observation of single-emitter circularly polarized fluorescence of definite handedness. The polarization selectivity is produced by a chiral microcavity. We also observed fluorescence antibunching from a colloidal CdSe QD in this microcavity. Earlier, we achieved both fluorescence antibunching [19–21] and definite *linear* polarization of single dye molecule fluorescence at room temperature in planar aligned nematic liquid crystal (LC) hosts. This method was applied for anisotropic dye molecules which can be aligned by rod-like nematic LC molecules [21,24]. A chiral microcavity provides circular polarized fluorescence for emitters even without dipole moments. Such a microcavity can be prepared from CLCs for any optical wavelength. We also present here chiral microcavities for PbSe QDs with a fluorescence maximum at 1.5 μm prepared both from monomeric

(fluid-like) and oligomeric glassy CLCs. By imaging the fluorescence of QDs in a 1.5-μm microcavity as well as in a polymer DBR microcavity with a defect layer we also demonstrate their potential for SPS device applications.

Section 2 of this paper describes the experimental setup for fluorescence imaging, antibunching and polarization measurements. Section 3 is devoted to chiral microcavities made of CLCs doped with single colloidal CdSe, CdSeTe or PbSe QDs. It contains details on sample preparation, photonic-bandgap transmission curves matched with QD fluorescence at 580 nm, 700 nm and 1.5 μm, circular polarized fluorescence, and antibunching measurements. Section 4 describes the preparation of a polymer microcavity with a defect layer doped with single CdSe QDs between the DBRs and single-QD fluorescence imaging in this structure.

2. Experimental setup

The experimental setup consists of a home-built confocal fluorescence microscope based on a Nikon TE2000-U inverted microscope with several output ports. Figure 1 shows the abbreviated schematics of our experiment for fluorescence imaging and antibunching measurements (*a*) and polarization and spectral measurement (*b*).

We excite our samples with 76 MHz repetition-rate, 6 ps pulse duration, 532-nm light from a Lynx mode-locked laser (Time-Bandwidth Products Inc.). To obtain a diffraction-limited spot on the sample, the excitation beam is expanded and collimated by a telescopic system with a spatial filter. The samples are placed in the focal plane of a 1.3-numerical
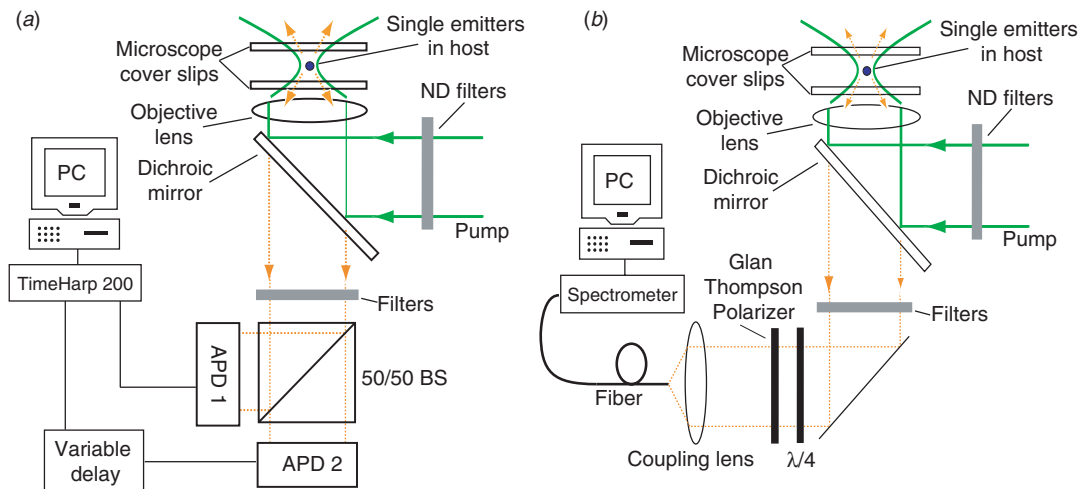

Figure 1. Schematics of experimental setup for fluorescence imaging and antibunching measurements (*a*); spectral and polarization measurements. (*b*) We used the following abbreviations: neutral density (ND); single-photon counting avalanche photodiode module (APD); beamsplitter (BS). (The color version of this figure is included in the online version of the journal.)

aperture, oil-immersion microscope objective used in confocal reflection mode. In focus, the intensities used are of the order of several $kW\,cm^{-2}$. Residual transmitted excitation light is removed by a dichroic mirror and a combination of two interference filters yielding a combined rejection of nine orders of magnitude at 532 nm. The sample's holder is attached to a piezoelectric, XY translation stage providing a raster scan of the sample through an area up to $50\,\mu m \times 50\,\mu m$.

The following diagnostics are placed in the separate output ports:

(1) A Hanbury Brown Twiss interferometer consisting of a 50/50 beamsplitter cube and two cooled, Si single photon counting avalanche photodiode modules (APDs) SPCM AQR-14 (Perkin Elmer). The time interval between two consecutively detected photons in separate arms is measured by a TimeHarp 200 time correlated single-photon counting card using a conventional start-stop protocol.

(2) Electron multiplying, cooled CCD-camera iXon DV 887 ECS-BV (Andor Technologies).

(3) Fiber-optical spectrometer (Ocean Optics). The method of defining the dissymmetry of circular polarization is described in [25]. For circular-polarization measurements both an achromatic quarter waveplate and a Glan Thompson linear polarizer on rotating mounts are placed in the spectrometer port in front of the spectrometer. An area with several single QDs is selected by an EM-CCD camera and/or APD-detectors with a raster-scan of the sample. It is imaged to the spectrometer input fiber. The spectra are recorded with a 6-s accumulation time with background subtraction.

CdSe/ZnS core/shell QDs were obtained commercially from Evident Technologies (maximum fluorescence wavelength $\lambda_o = 620$ nm) or were synthesized according to published methods ($\lambda_o = 580$ nm) [26,27]. CdSeTe QDs ($\lambda_o = 700$ nm) were obtained commercially from Invitrogen. $PbSe/C_{18}H_{34}O_2$ QDs ($\lambda_o = 1.5\,\mu m$) containing PbSe QDs of smaller-size ($\lambda_o \sim 900$ nm) were synthesized according to variations of literature methods [28,29].

3. Chiral microcavity made of LCs doped with single colloidal QDs

3.1. CLC sample preparation

In a planar-aligned CLC, the rod-shaped anisotropic molecules with small chiral 'tails' form a periodic helical structure with pitch p [30]. For sufficiently thick CLC layers, the reflectance of normally incident, circularly polarized light, with the same handedness as the CLC structure, is nearly 100% within a band centered at $\lambda_c = n_{av}p$. The bandwidth is approximately $\Delta\lambda = \lambda_c \Delta n/n_{av}$, where n_{av} is the average of the ordinary n_o and extraordinary n_e refractive indices of the medium: $n_{av} = (n_o + n_e)/2$, and $\Delta n = n_e - n_o$. This periodic structure can also be viewed as a 1-D photonic crystal, with a bandgap within which propagation of light is forbidden. For emitters located within this structure, the spontaneous emission rate is suppressed within the spectral stopband and enhanced near the *band edge* [31,32]. Lasing experiments in dye-doped CLC structures with high dopant concentration [32] confirmed that the best condition for coupling is when the dopant fluorescence maximum is at a band edge of the CLC selective transmission curve.

For sample preparation we use two types of LCs: (1) *monomeric* mixtures of low-molecular-weight E7 nematic-LC blend with a chiral additive CB15 and (2) oligomer CLC (OCLC) powders [19–20]. E7 and CB15 are fluids at room temperature. Both materials were supplied by EM Industries. We filtered the E7 and CB15 to remove fluorescent contaminants. Powder OCLCs were supplied by Wacker GmbH.

For development of CLC hosts which form a chiral photonic bandgap tuned to the QD fluorescence band, two main aspects are important: (1) properly choosing the concentration (or ratio) of different LC components and (2) providing planar alignment of the CLC. For the monomeric mixtures, the stopband position λ_c of the photonic bandgap is defined roughly by $C = n_{av}/(\lambda_c \times HTP)$, where C is the weight concentration of CB15 in the CB15/E7 mixture, $n_{av} \sim 1.6$ for this mixture, and $HTP \sim 7.3\,\mu m^{-1}$ is the helical twisting power of the chiral additive in nematic liquid crystal. The actual stopband position relative to the fluorescence maximum of the QD was further defined empirically by obtaining selective transmission curves of different samples using a spectrophotometer. After monomeric CLC preparation, a QD solution of ~ 1nM concentration was mixed with monomeric CLC and solvent was evaporated.

For the OCLC powders there is not such a simple relation between the concentration and λ_c. We found the right ratio R of components only empirically by mixing the different ratios of two OCLC with different λ_c (1.17 μm and 2.15 μm) by dissolving them in a solvent. By evaporating the solvent using a procedure of heating this solution in a vacuum inside a rotating retort, we obtained a new powder oligomer with an intermediate λ_c.

After that, monomeric CLC doped with QDs is placed between two cover glass slips and planar aligned through uni-directional mechanical motion between

the two slides. For planar alignment of OCLC, a cover slip with Wacker powder is placed on a hot plate and melted at ~120°C. The second slip is used to shear the melted oligomer at this temperature. After the alignment the sample is slowly cooled into the glassy state, preserving CLC order and planar alignment [20]. For single-molecule fluorescence experiments Wacker powders need to be purified. For further details of CLC doping and sample preparation from both monomeric and oligomeric LCs with different photonic bandgaps, see [19,20].

3.2. 1-D-photonic bandgap transmission curves

By properly choosing the concentration of different LC monomers and/or Wacker glassy oligomers and providing planar alignment of the LCs, we developed CLC chiral 1-D photonic bandgap structures with

different stopband positions doped with single QDs (either CdSe, CdSeTe or PbSe). In both cases of monomeric and oligomeric liquid crystals, increasing the concentration (or ratio) of a component with higher HTP changes the position of the stopband in the direction of shorter wavelengths. The error in defining weight concentrations can smear this effect for mixtures with concentrations close to one another. The stopband positions are tuned to the QD fluorescence bands for the visible (Figure 2) and ~1.5 μm (Figure 3).

Figure 2 shows selective transmission of two monomeric 1-D chiral photonic bandgap structures with 36.6% (*a*) and 36.0% (*b*) weight concentrations of chiral additive CB15 in E7/CB15 mixtures. It also shows the fluorescence spectra of the CdSe (*a*) and CdSeTe (*b*) QDs with the centers of the fluorescence peaks near 580 and 700 nm.
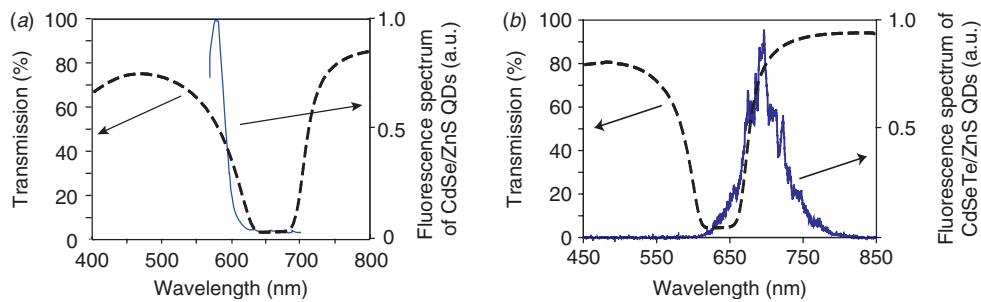

Figure 2. Selective transmission of two monomeric chiral photonic bandgap CLC hosts for right-handed circular polarized light and the fluorescence spectrum of the CdSe (*a*) and CdSeTe (*b*) QDs. (The color version of this figure is included in the online version of the journal.)

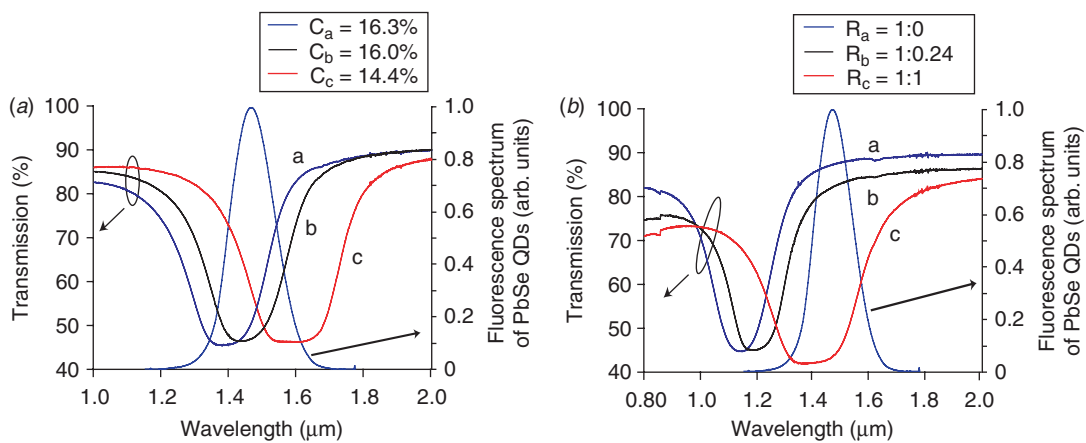
Figure 3. PbSe QD fluorescence spectrum and selective transmission of chiral photonic bandgap cholesteric microcavities for telecom wavelength 1.5 μm for *unpolarized* light [for circularly polarized light the minimum transmission value will be smaller than 5% (see Figure 2, where measurements were made with a linear polarizer and achromatic quarter waveplate)]. (*a*) For monomeric liquid crystals of different concentrations, C, of chiral additive CB15 in CB15 and E7 mixture; (*b*) for Wacker chiral oligomeric powder mixtures of different ratios, R, of $\lambda_c = 1.17$ μm powder to $\lambda_c = 2.15$ μm powder. (The color version of this figure is included in the online version of the journal.)

Figure 3 shows spectral transmission curves for several prepared photonic bandgap structures with the band edge at 1.5 μm made of monomeric CLC (left) and OCLC (right). The fluorescence spectrum of a PbSe QD solution at high QD concentration is depicted in both figures.

3.3. Circular polarized fluorescence and antibunching in a chiral microcavity

Figure 4(a), shows several single-CdSe/ZnS QD fluorescence images in a CLC host with the same QD fluorescence spectrum as presented in Figure 2(a). The spectral transmission of this CLC photonic bandgap structure is similar to the spectral transmission curve also shown in Figure 2(a). Note that the dark horizontal stripes in the pattern of separate QDs are the result of single QD blinking, which is a characteristic property of single-QD fluorescence. The raster scan area is 15 μm × 15 μm. Figure 4(b), shows single-PbSe QD fluorescence images in a CLC photonic bandgap structure with the spectral transmission curve (a) in Figure 3(a). We used the
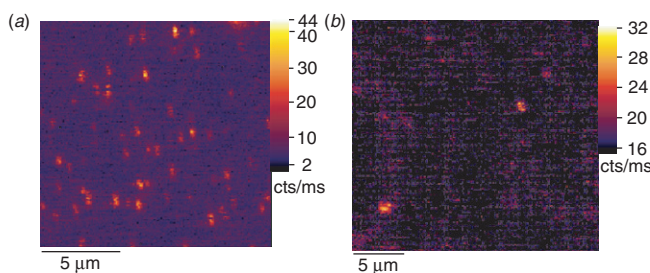
solution containing both 1.5 μm emitting QDs and a small concentration of 900 nm emitting QDs as a result of synthesis. Using Si APDs we are only able to record QD fluorescence from the smaller size QDs with $\lambda_o \sim 900$ nm.

Figure 5(b) shows emission spectra for CdSe/ZnS QDs in a chiral CLC cavity for right-handed (black line) and left-handed circular polarizations (red line). The spectral transmission of the cavity is presented in Figure 2(a). The degree of circular polarization is measured by the dissymmetry factor g_e [25,33]:

$$g_e = \frac{2(I_L - I_R)}{(I_L + I_R)}, \qquad (1)$$

where I_L and I_R are the intensities of left-handed and right-handed circular polarizations.

At 580 nm, $g_e = -1.6$. For unpolarized light $g_e = 0$. The fluorescence spectrum of the same CLC microcavity without QDs is depicted in Figure 5(a). The nature of the spectral peaks which were observed in the CLC cavity without QDs is unclear. It is not a microcavity effect, because we observed the same features from unaligned CLC without a microcavity. It can be attributed to some impurities which we did not remove during the LC purification procedure.

We also illuminated a single CdSe QD in the CLC host and measured the fluoresced photon statistics under saturation conditions. Figure 6(a) presents the $g^{(2)}(t)$ histogram at different interphoton times t. The value of $g^{(2)}(0)$ is 0.76 ± 0.04. One sees that the peak at zero interphoton time is clearly smaller than any of the other peaks, which shows an antibunching property. This antibunching histogram can be improved by using QDs which fluoresce outside the fluorescence spectrum of the CLC shown in Figure 5(a). One easily can see a host fluorescence peak at the fluorescence maximum of the selected QD. At wavelengths larger than $\sim$700 nm, no host background is observed.

Figure 4. Typical confocal fluorescence images (1) of single CdSe QDs in CLC host (a) (15 μm × 15 μm scan), and single PbSe QDs in CLC host (25 μm × 25 μm scan) (b). (The color version of this figure is included in the online version of the journal.)
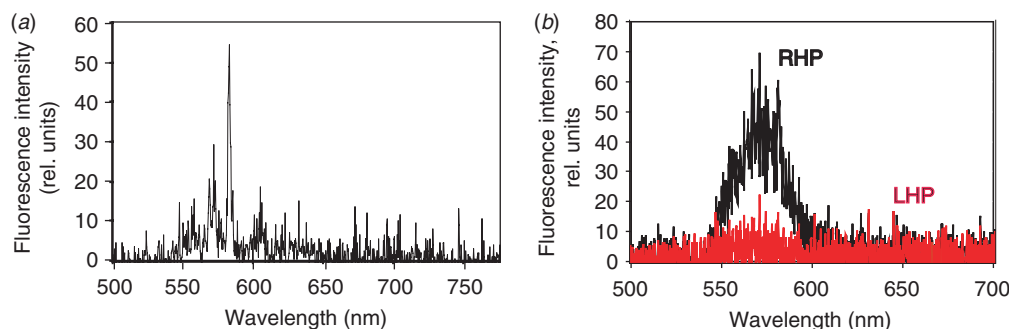

Figure 5. Fluorescence spectrum of the monomeric CLC host without QDs (a) and CdSe QDs in a similar CLC host (Figure 2(a)) for two different circular polarizations of single photons: (b) black line – right-handed, red line – left-handed. (The color version of this figure is included in the online version of the journal.)
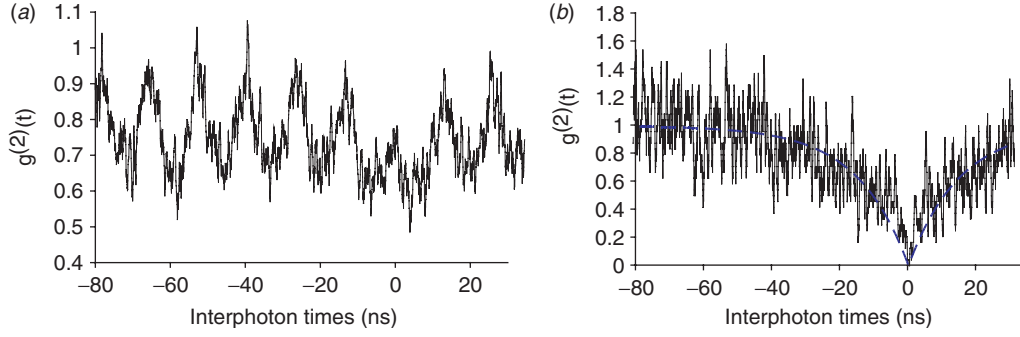
Figure 6. Histograms of coincidence counts of single-QD fluorescence in a CLC host under pulsed excitation. The dip at zero interphoton time indicates antibunching. (*a*) For the CdSe QD of Figure 2(*a*) with λ_0 inside the liquid crystal background; (*b*) for CdSeTe QD of Figure 2(*b*) with λ_0 outside the liquid crystal background. (The color version of this figure is included in the online version of the journal.)

We doped CdSeTe QDs with $\lambda_0 = 700$ nm in the CLC host with the stopband shown in Figure 2(*b*), and when illuminating a single QD, obtained antibunching with $g^{(2)}(0) \sim 0$ (Figure 6(*b*)). Note that the QD fluorescence maximum is outside of the CLC background spectrum. It shows that excluding the CLC background helps to obtain better antibunching. The fitted curve $g^{(2)}(t) = 1 - (1/N)e^{(-t/\tau)}$ [34] gives $g^{(2)}(0) = 0.001 \pm 0.034$, with a fluorescence lifetime $\tau \sim 15$ ns and with the number N of illuminated emitters equal to 1. This quantum dot has τ larger than the time between two laser pulses, so we cannot observe fluorescence excited by the separate laser pulses as in Figure 6(*a*).

Estimation of the efficiency P of *on-demand polarized* antibunched photon emission into the collecting objective showed $P \sim 10\%$ with the second-order correlation function $g^{(2)}(0) = 0.8$, measured from the antibunching histogram of Figure 6 (*a*), using $5.2\,\mu$W excitation power. We define P from the following equation:

$$[1 - g^{(2)}(0)]N_{\text{out}} = N_{\text{incQD}}\alpha\beta Q_{\text{APD}}GP, \qquad (2)$$

where $N_{\text{out}} = 2 \times 10^5$ counts s^{-1} is the measured photon count rate by the APDs and $N_{\text{incQD}} = N_{\text{inc}}\sigma_{\text{abs}} = (I/h\nu)\sigma_{\text{abs}} = 7.17 \times 10^6$ photons s^{-1} is the number of photons incident on the quantum dot per second. Here I is the measured incident intensity in the focal area of the sample ($I = 2.23$ kW cm^{-2}), $h\nu = 3.73 \times 10^{-19}$ J for 532-nm light, and $\sigma_{\text{abs}} = 1.2 \times 10^{-15}$ cm^2 is the absorption cross-section of the quantum dot at 532 nm taken from the measurements of Leatherdale et al. [35].

The parameters of Equation (2) defining losses in the microscope detection system ($\alpha\beta Q_{\text{APD}}$) are as follows: $\alpha = 0.49$ is the measured transmission of all interference and colored glass filters in front of the APDs (preventing cross-talk between them), $\beta = 0.48$ is the measured transmission of the objective, microscope optics, imaging lenses and nonpolarizing beamsplitter, and $Q_{\text{APD}} = 0.58$ is the quantum efficiency of the APD at 580 nm as quoted by the vendor.

The parameter $G = 0.4$ is the measured CdSe/ZnS QD quantum yield. The value of P characterizes the cavity (collection efficiency from the source into the collecting objective), and the value of GP characterizes both the cavity and the fluorescent emitter together. In our measurements for the *on-demand polarized* antibunched photon source, $P \sim 10\%$, and $GP \sim 4\%$. The value of GP can be increased to 10% by using a quantum dot with $G \sim 1$ (see, e.g. experimental paper [36]).

4. Polymer microcavity with defect layer doped with single QDs between the DBRs

The second type of photonic bandgap structure doped with single CdSe/ZnS core/shell QDs from Evident Technologies is prepared using solution processing. The fluorescence maximum of these QDs is $\sim$620 nm. The details of structure preparation are reported in [22–23]. The DBRs are fabricated by spin coating alternating quarter wavelength thick polymer layers with different refractive indices n [poly-vinylcarbazole (PVK) with $n = 1.683$ and poly-acrylic acid (PAA) with $n = 1.428$ at 600 nm] [22,23]. Solvents are chosen such that the solvent for one polymer does not dissolve the other polymer. PVK is soluble in non-polar solvents such as toluene or chlorobenzene but not in polar solvents such as water or alcohol, whereas PAA is soluble in alcohol but not in chlorobenzene. Greater than 90% reflectivity is obtained using 10 periods of the DBR structure.

The 1-D microcavity is formed by sandwiching a λ/n_{PVK} thickness PVK defect layer doped with single QDs between two such DBRs. The top and bottom DBRs both comprise 10 periods. QDs are mixed with a defect layer PVK polymer solution and spin coated
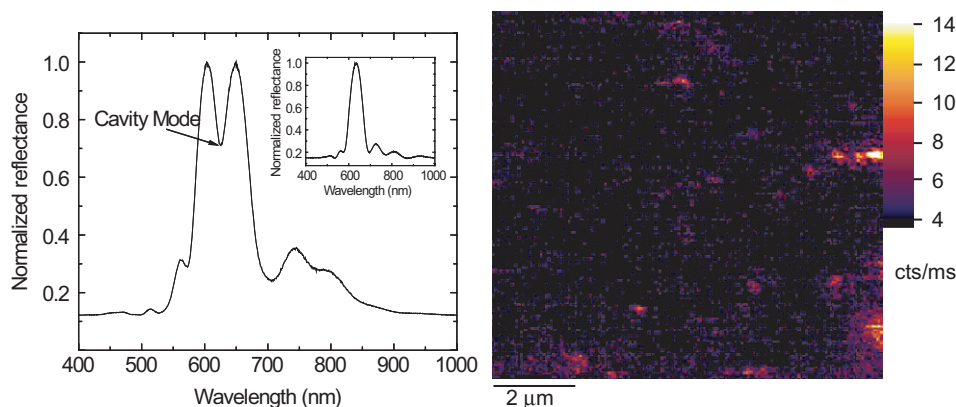
Figure 7. (*a*) Reflectivity spectrum of the polymeric microcavity embedded with CdSe QDs with $\lambda_0 = 620$ nm. Shown in the inset is the normalized reflectivity spectrum showing the stop band of the ten-period Bragg reflector without the defect layer. (*b*) Single QD fluorescence imaging in a polymeric microcavity under 532-nm excitation (10 µm × 10 µm scan). (The color version of this figure is included in the online version of the journal.)

onto the bottom DBR structure (QD concentration in solution is ~7.7 nM).

Figure 7(*a*) shows the reflectivity of the whole structure (DBRs with a defect layer between them) with the cavity mode at ~620 nm. The quality factor (*Q*) of such a microcavity was found to be ~40. The theoretical estimate of Q for the polymer distributed Bragg mirrors to form a microcavity structure is within the same order of magnitude (~60). This discrepancy is attributed to lower reflectivities of the actually fabricated DBR mirrors than anticipated by the theory using the ideal mirrors.

The inset of Figure 7(*a*), shows the normalized reflectivity spectra of the DBR with 10 periods without any defect layer. Fluorescence imaging of single QDs in a DBR structure with a defect layer is shown in Figure 7(*b*). This raster scan image shows blinking of single QDs (bright horizontal stripes) and a low host fluorescence background, making these structures suitable for single photon source applications.

It was reported earlier for a high concentration of CdSe/ZnS QDs [22,23] that the photoluminescence decay time τ of the QDs in a microcavity was ~150 ps. For QDs on a bare glass substrate or embedded in PVK without a bandgap structure τ was found to be ~1000 ps and ~400 ps, respectively [22,23].

It should be noted that this type of microcavity provides 1-D light confinement so that light can propagate in a lateral direction. Preparation of a micropillar microcavity from the current 1-D microcavity using focused ion beam etching is in progress. Etching with a similar 1-D microcavity was carried out in [11]. An elliptical cross-section micropillar will provide linear polarized emission of desired direction from single colloidal QDs. In contrast to [10], in which DBRs and a defect layer doped with colloidal QDs between them are prepared by sputtering

alternating SiO_2 and TiO_2 layers, the process described here is more simple and robust and compatible with the standard solution processing technique of colloidal QDs. The technique of sputtering and/or thermal evaporation require multiple deposition systems – one for colloidal quantum dots and another for DBRs. In addition, these techniques have detrimental effects on the optical properties of the QDs due to the introduction of surface defects.

5. Conclusion

Single semiconductor nanocrystal (colloidal QD) fluorescence in microcavities was studied for the first time. We report the first observation of single-emitter circularly polarized fluorescence of definite handedness due to microcavity chirality. The chiral microcavities were prepared by a simple method of planar alignment of cholesteric liquid crystals. Antibunching experiments show that the fluorescence background of the medium is low, so that antibunching of QD fluorescence is preserved. 1-D chiral photonic bandgap structures possess an advantage over conventional 1-D photonic bandgap technologies. Because the refractive index *n* varies gradually rather than abruptly in chiral structures, there are no losses into the waveguide modes, which arise from total internal reflection at the border between two consecutive layers with different *n*. Therefore, it is not necessary to make a micropost structure as in [11] to reject 'leaky' modes in a lateral direction. In addition, liquid crystal microcavities are wavelength-tunable by changing the temperature and applied electric field.

Single QD fluorescence in a polymer microcavity with a defect layer doped with single QDs between DBRs was studied as well. Such easily prepared and

robust organic microcavities using low fluorescence background materials can be incorporated in visible and telecom SPSs.

Our next steps will be to increase the efficiency of our on-demand polarized antibunched photon source. We will do this by: (1) selecting QDs with $G \sim 100\%$, λ_o outside the host fluorescence background, and τ shorter than several ns, and (2) providing strong coupling between a single QD and a cavity by refining the cavity preparation technique. We also plan to demonstrate fluorescence antibunching at telecom wavelength.

Acknowledgements

References

[1] *New J. Phys.*, special issue, Focus on Single Photons on Demand, **2004**, 6.

[2] Kumar, P.; Kwiat, P.; Migdall, A.; Nam, S.W.; Vuckovic, J.; Wong, F.N.C. *Quantum Information Processing* **2004**, 3, 215–231.

[3] Lounis, B.; Orrit, M. *Rep. Progr. Phys.* **2005**, 68, 1129–1179.

[4] Yamamoto, Y.; Santori, Ch.; Vuskovic, J.; Fattal, D.; Waks, E.; Diamanti, E. *Progr. Informatics* **2005**, 1, 5–37.

[5] Lounis, B.; Bechtel, H.A.; Gerion, D.; Alivisatos, P.; Moerner, W.E. *Chem. Phys. Lett.* **2000**, 329, 399–404.

[6] Messin, G.; Hermier, J.P.; Giacobino, E.; Desbiolles, P.; Dahan, M. *Opt. Lett.* **2001**, 26, 1891–1893.

[7] Huang, H.; Dorn, A.; Bulovic, V.; Bawendi, M. *Appl. Phys. Lett.* **2007**, 90, 023110-1–13.

[8] Vahala, K.J. *Nature* **2003**, 424, 839–846.

[9] Englund, D.; Fattal, D.; Walks, E.; Solomon, G.; Zhang, B.; Nakaoka, T.; Arakawa, Y.; Yamamoto, Y.; Vuckovic, J. *Phys. Rev. Lett.* **2005**, 95, 013904-1–7.

[10] Poitras, M.; Lipson, C.B.; Du, H.; Hahn, M.A.; Krauss, T.D. *Appl. Phys. Lett.* **2003**, 82, 4032–4034.

[11] Kahl, M.; Thomay, T.; Kohnle, V.; Beha, K.J; Merlein, K.; Hagner, M.; Halm, A.; Ziegler, J.; Nann, T.; Fedutik, Y.; Woggon, U.; Artemyev, M.; Pérez-Willard, F.; Leitenstorfer, A.; Bratschitsch, R. *Nano Lett.* **2007**, 7, 2897–2900.

[12] Martiradonna, L.; De Giorgi, M.; Troisi, L.; Carbone, L.; Gigli, G.; Cingolani, R.; De Vittorio, M. *International Conference on Transparent Optical Networks (ICTON)* **2006**, 2, 64–67.

[13] Lodahl, P.; Floris van Driel, A.; Nikolaev, I.S.; Irman, A.; Overgaag, K.; Vanmaekelbergh, D.; Vos, W.L. *Nature* **2004**, 430, 654–657.

[14] Fushman, I.; Englund, D.; Vuckovic, J. *Appl. Phys. Lett.* **2005**, 87, 241102-1–23.

[15] Wu, Z.; Mi, Z.; Bhattacharya, P.; Zhu, T.; Xu, J. *Appl. Phys. Lett.* **2007**, 90, 171105-1–3.

[16] Bose, R.; Yang, X.; Chatterjee, R.; Gao, J.; Wong, C.W. *Appl. Phys. Lett.* **2007**, 90, 111117-1–3.

[17] Hoogland, S.; Sukhovarkin, V.; Howard, I.; Cauchi, S.; Levina, L; Sargent, E.H. *Opt. Express* **2006**, 14, 3273–3281.

[18] Barrelet, C.J.; Bao, J.; Loncar, M.; Park, H.-G.; Capasso, F.; Lieber, C.M. *Nano Lett* **2006**, 6, 11–15.

[19] Lukishova, S.G.; Schmid, A.W.; McNamara, A.J.; Boyd, R.W.; Stroud Jr, C.R. *IEEE J. Selected Topics in Quant. Electron* **2003**, 9, 1512–1517.

[20] Lukishova, S.G.; Schmid, A.W.; Supranowitz, C.M.; Lippa, N.; McNamara, A.J.; Boyd, R.W.; Stroud Jr, C.R. *J. Mod. Opt.* **2004**, 51, 1535–1547.

[21] Lukishova, S.G.; Schmid, A.W.; Knox, R.P.; Freivald, P.; McNamara, A.; Boyd, R.W.; Stroud Jr, C.R.; Marshall, K.L. *Molec. Cryst. Liq. Cryst.* **2006**, 454, 403–416.

[22] Valappil, N.V.; Zeylikovich, I.; Gayen, T.; Das, B.B.; Alfano, R.R.; Menon, V.M. *MRS Fall Meeting*, Boston **2006**, Paper no. M10.1.

[23] Valappil, N.; Luberto, M.; Menon, V.M.; Zeylikovich, I.; Gayen, T.K.; Franco, J.; Das, B.B.; Alfano, R.R. *Photon. Nanostruct.* **2007**, 5, 184–188.

[24] Lukishova, S.G.; Schmid, A.W.; Knox, R.; Frievald, P.; Bissell, L.; Boyd, R.W.; Stroud, C.R. *J. Mod. Opt.* **2007**, 54, 417–429.

[25] Shi, H.; Conger, B.M.; Katsis, D.; Chen, S.H. *Liquid Crystals* **1998**, 24, 163–172.

[26] Murray, C.B.; Norris, D.J.; Bawendi, M.G. *J. Am. Chem. Soc.* **1993**, 115, 8706–8715.

[27] Qu, L.; Peng, Z.A.; Peng, X. *Nano Lett.* **2001**, 1, 333–337.

[28] Murray, C.B.; Sun, S.; Gaschler, W.; Doyle, H.; Betley, T.A.; Kagan, C.R. *IBM J. Res. Devel.* **2001**, 45, 47–55.

[29] Du, H.; Chen, C.; Krishnan, R.; Krauss, T.D.; Harbold, J.M.; Wise, F.W.; Thomas, M.G.; Silcox, J. *J. Nano Lett.* **2002**, 2, 1321–1324.

[30] Chanrasekhar, S. *Liquid Crystals;* Cambridge University Press: London, 1977.

[31] Dowling, J.P.; Scalora, M.; Bloemer, M.J.; Bowden, C.M. *J. Appl. Phys* **1994**, 75, 1896–1899.

[32] Kopp, V.I.; Fan, B.; Vithana, H.K.M.; Genack, A.Z. *Opt. Lett.* **1998**, 23, 1707–1709.

[33] Chen, S.H.; Katsis, D.; Schmid, A.W.; Mastrangelo, J.C.; Tsutsui, T.; Blanton, T.N. *Nature* **1999**, 397, 506–508.

[34] Hollars, C.W.; Lane, S.M.; Huser, T. *Chem. Phys. Lett.* **2003**, 370, 393–398.

[35] Leatherdale, C.A.; Woo, W.-K.; Mikulec, F.V.; Bawendi, M.G. *J. Phys. Chem. B* **2002**, 106, 7619–7622.

[36] Yao, J.; Larson, D.R.; Vishwasrao, H.D.; Zipfel, W.R.; Webb, W.W. *Proc. Natl. Acad. Sci.* **2005**, 102, 14284–14289.